

Hexameric Palladium(II) Terpyridyl Metallomacrocycles: Assembly with 4,4'-Bipyridine and Characterization by TWIM Mass Spectrometry**

Sujith Perera, Xiaopeng Li, Monica Soler, Anthony Schultz, Chryst Wesdemiotis,*
Charles N. Moorefield, and George R. Newkome*

The construction of 2D or 3D materials using supramolecular chemistry principles has become an intriguing area of research. In particular, terpyridine-based building blocks have played a pivotal role in the construction of dimers,^[1,2] triangles,^[3–5] trigonal prisms,^[6] squares,^[4,5,7–9] pentagons,^[10] and hexagons,^[11–13] based on their planar tridentate coordination mode^[4,5,12] and their facile potential for modification.^[14] Terpyridine (terpy) and its metal complexes are also of interest because of their well-known photophysical and electronic properties.^[15] Thus, the use of terpyridine for the construction of materials and molecular architectures with increasing complexity will continue to mature.

However, the difficulty of obtaining single crystals suitable for X-ray structure determination means that other reliable techniques are essential for the characterization of macromolecular structures. Electrospray ionization (ESI) mass spectrometry has been applied in the identification and characterization under mild ionization conditions.^[16] In particular, the cold-spray (CSI) technique reported by Fujita and co-workers,^[16d,e] and the Fourier transform mass spectrometry (FTMS) technique developed by Schalley and co-workers^[16f,g,h] are the most prominent ESI-based methods. The work of Piguet and co-workers^[16i] is also notable. Unfortunately, the signals that correspond to different

charge states are superimposed and only a few isotope patterns of different charge states can be deconvoluted. Recently, traveling wave ion mobility mass spectrometry (TWIM-MS),^[17] a variant of ion mobility mass spectrometry (IM-MS), has been successfully applied to the detection and characterization of supramolecules.^[18] Ion-mobility-based separation enhances the resolving power of mass spectrometry by adding shape- and charge-dependent dispersion, which reduces isomer superposition and can deconvolute the isotope patterns of different charge states.^[18] Notably, isomeric linear and cyclic structures have been separated based on their different drift time in the ion mobility device.

Herein, we report the 4,4'-bipyridine (bpy) assisted assembly of a hexagonal, dodeca Pd^{II} terpyridyl based macrocycle, and its characterization by NMR and TWIM-MS. A recent example of the use of terpyridine and its Pd coordination for the formation of a metallocyclic rectangle was reported by Bosnich and co-workers,^[7] whereby two cofacially oriented, Pd^{II} terpyridine MeCN adducts were dimerized upon the addition of 4,4'-bipyridine. Our synthetic efforts began with an improved preparation of 1,3-bis(2,2':6',2''-terpyridin-4'-yl)-5-*tert*-butylbenzene^[19] (**1**), which was isolated in 60% yield and exhibited identical ¹H and ¹³C NMR spectra to that of the initially reported ligand.^[19]

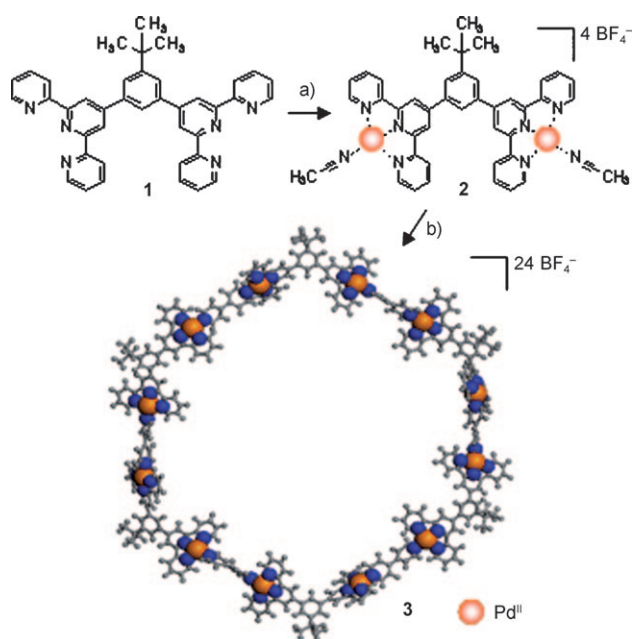
Ligand **1** was prepared by the reduction of commercially available 5-*tert*-butylbenzene-1,3-dicarboxylic acid with BH₃·THF, followed by selective oxidation with pyridinium chlorochromate (PCC) and subsequent grinding with 2-acetylpyridine (4.05 equivalents) and NaOH to give an orange solid, which was then added to NH₄OH and EtOH and heated at reflux for 24 hours. This ligand, which has coordination sites that are positioned 120 degrees apart, was treated with [Pd^{II}(MeCN)₄](BF₄)₂ in dry MeCN to give [(1,3-bis(2,2':6',2''-terpyridin-4'-yl)-5-*tert*-butylbenzene)Pd₂(MeCN)₂](BF₄)₄ **2** in nearly quantitative yield (Scheme 1). Ligand **1** was initially insoluble in MeCN, but was readily solubilized when treated with [Pd^{II}(MeCN)₄](BF₄)₂ in MeCN. The ¹H NMR data confirmed the formation of adduct **2**, with signals at δ = 8.68 (s, 3',5'-terpyH), 8.63–8.58 (m, 6,6''-terpyH and 3,3''-terpyH), 8.49 (t, 4,4''-terpyH), and 7.89 ppm (t, 5,5''-terpyH); see Figure 1. A downfield shift of the *tert*-butyl singlet peak (from δ = 1.51 to 1.57 ppm, Δδ = 0.06 ppm) and the IR absorptions observed at 2334 and 2304 cm⁻¹ assigned to the C≡N stretch^[20] also support the formation of a Pd^{II} adduct **2**.

[*] Dr. S. Perera,^[+] Dr. X. Li,^[+] Dr. M. Soler, A. Schultz, Prof. Dr. C. Wesdemiotis, Dr. C. N. Moorefield, Prof. Dr. G. R. Newkome
Department of Polymer Science, Department of Chemistry,
The University of Akron
302 Buchtel Common, Akron, OH 44325 (USA)
Fax: (+1) 330-972-2368
E-mail: wesdemiotis@uakron.edu
newkome@uakron.edu
Homepage: <http://www.dendrimers.com>

[†] These authors contributed equally to this work.

[**] We thank the National Science Foundation for generous financial support (grant nos. CHE-0517909 and 0833087 to C.W., no. DMR-0705015 to G.R.N., and no. DMR-0821313 for the purchase of the instrument for the TWIM-MS studies). We gratefully acknowledge the expertise of Dr. Mingming Guo, Solid State NMR Manager at The University of Akron for his help with the 2D-DOSY NMR experiments. We are grateful to Dr. Thomas Wyttenbach and Prof. Michael T. Bowers for helpful discussions on collision cross sections in ion-mobility experiments. TWIM = traveling wave ion mobility.

 Supporting information (synthesis and characterization of the ligands and complexes) for this article is available on the WWW under <http://dx.doi.org/10.1002/anie.200906198>.



Scheme 1. Assembly of the palladium hexamer **3** represented by a computer-generated, partial space-filling model; reagents and conditions: a) MeCN, $[\text{Pd}(\text{MeCN})_4](\text{BF}_4)_2$, 4 h, 25 °C; b) MeCN, 4,4'-bipyridine (1 equiv), 1 h, 25 °C. C gray, N blue, Pd^{II} orange.

Based on the lability of weak ligands such as NO_3^- , OTf^- , and MeCN,^[7] the addition of one equivalent of 4,4'-bipyridine to bis(Pd^{II} terpyridine) adduct **2** in MeCN leads to the self-assembly of the dodeca Pd^{II} metallomacrocycle **3** (Scheme 1). Evidence for structure **3** in the ¹H NMR spectrum includes the observation of a small downfield shift of the singlet assigned to the *tert*-butyl group (from $\delta = 1.57$ to 1.61 ppm, $\Delta\delta = 0.04$ ppm), and a sharp singlet ($\delta = 8.68$ ppm, 3',5'-terpyHs) indicative of the symmetric, cyclic structure. An expected downfield shift of the 6,6''-terpyHs ($\delta = 8.61$ to 8.95 ppm, $\Delta\delta = 0.34$ ppm) and the presence of the 4,4'-bipyridine proton absorptions ($\delta = 8.46$ and 7.71 ppm), as well as a signal at m/z 3174 in the ESI mass spectrum, further confirmed the structure of **3**. Notably, the symmetry observed in the ¹H and ¹³C NMR spectra eliminates the possibility of oligomeric products with uncomplexed terpyridine moieties, which, if present, could easily be detected above the sensitivity limits of the NMR.

To further establish the ease of displacement of the MeCN ligand from the coordination sphere, adduct **2** was treated with two equivalents of 4-*tert*-butylpyridine to produce the model biscomplex **4** (Scheme 2). As expected, this reaction produced a compound with two different *tert*-butyl groups in a 1:2 ratio, which arises from the bis(terpyridine) and 4-*tert*-butylpyridine moieties. This assignment was confirmed by ¹H NMR spectroscopy, which showed C(CH₃)₃ signals at $\delta = 1.61$ and 1.47 ppm, respectively. Furthermore, the chemical shift ($\delta = 1.61$ ppm) of the *tert*-butyl groups on the macrocycle **3** mirrors that of the bis(terpyridine) *tert*-butyl moiety of **4**. Notably, temperature-dependent ¹H NMR experiments exhibited sharpened signals and confirmed that the broadened signals observed for **4** arise from a single

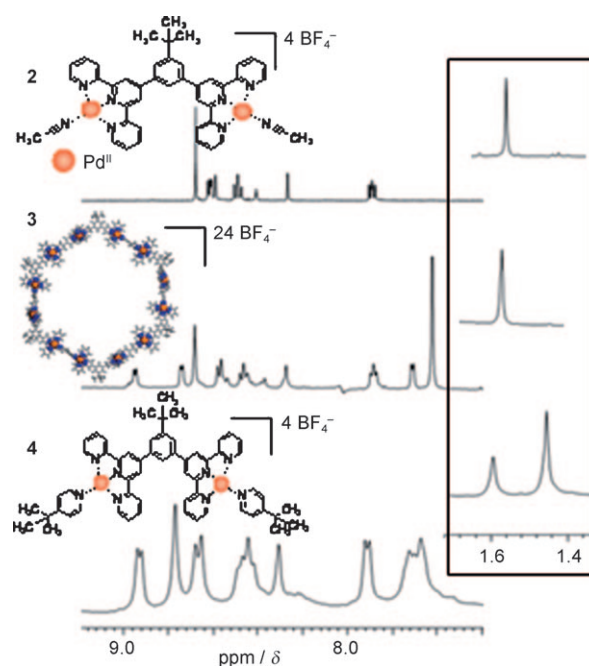
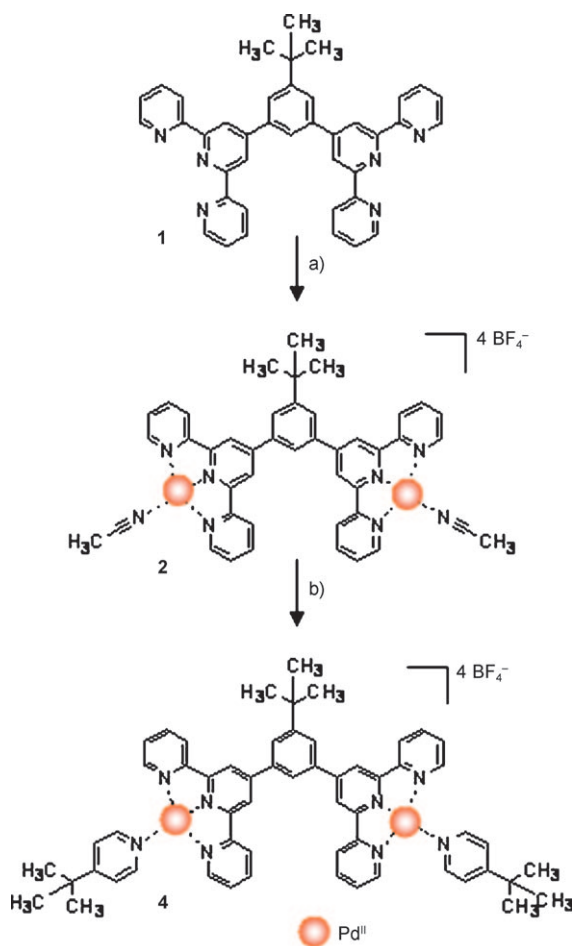


Figure 1. ¹H NMR spectrum (CD_3CN) of complexes **2**, **3**, and **4** showing the aromatic and *tert*-butyl regions. Orange spheres = Pd^{II}.

molecule (see page S8 in the Supporting Information^[S11]). The COSY and ¹³C NMR spectra of the adduct **2**, and macrocycles **3** and **4** also further verified the peak assignments and support the structures (see pages S10–S11 in the Supporting Information).

The full mass spectrum of the hexagonal dodeca Pd^{II} metallomacrocycle **3** (Figure S1 in the Supporting Information) is complicated for a multitude of reasons, which are discussed in detail in the Supporting Information. Briefly, 1) the large number of Pd isotopes gives rise to broad isotope patterns that extend over a wide m/z range; 2) the macrocycle **3** contains 24 BF_4^- counterions, which can lead to several different charge states in ESI, depending on the number of BF_4^- ions lost; 3) the remaining BF_4^- ions may undergo loss of BF_3 during the mass spectrometry experiment to form F^- counterions; and 4) linear fragments with different charges and BF_4^-/F^- content can be generated in the mass spectrometer. To address these problems, the ions at m/z 3174 were mass-selected and subjected to IM separation. Additionally, tandem mass spectrometry (MS/MS) was employed after IM separation to further characterize the different components of m/z 3174.

Based on the calculated m/z values, the ions at m/z 3174 can be either cyclic $[6\text{L}_1 + 12\text{Pd} + 6\text{L}_2]^{2+}$ ($\text{L}_1 = \mathbf{1}$ and $\text{L}_2 = 4,4'$ -bipyridine) with 20 F^- and 2 BF_4^- counterions, or linear $[3\text{L}_1 + 6\text{Pd} + 3\text{L}_2]^+$ with 10 F^- and 1 BF_4^- counterions. Three species are detected after ion mobility separation (Figure 2). Analysis of the corresponding isotope patterns reveals that the signal with a drift time of 13.85 ms represents singly charged ions (isotope spacing $\Delta m = 1.0$ Da) from the linear $[3\text{L}_1 + 6\text{Pd} + 3\text{L}_2]^+$ ion; whereas, the signal at 7.87 ms arises from ions with an isotope spacing of $\Delta m = 0.5$ Da and



Scheme 2. Synthesis of the palladium model complex **4**; reagents and conditions a) MeCN, $[\text{Pd}(\text{MeCN})_4](\text{BF}_4)_2$, 4 h, 25 °C; b) MeCN, 4-*tert*-butylpyridine (2 equiv), 1 h, 25 °C. Orange spheres = Pd^{II} .

corresponds to the doubly charged $[6\text{L}_1 + 12\text{Pd} + 6\text{L}_2]^{2+}$ ion. The isotope cluster of the signal at 5.90 ms was not well-resolved; the pattern of BF_3 losses upon MS/MS in the transfer cell, which is a collision cell following the IM region, indicates a +3 charge state for this component, which could result from aggregation of lower charge states.

Considering that the cyclic $[6\text{L}_1 + 12\text{Pd} + 6\text{L}_2]$ structure is the major product according to the NMR data (see Figure 1), and that the bis(terpyridine) **1** readily self-assembles with divalent transition metals to form metallomacrocycles,^[19] the signal at 7.87 ms is consistent with the assignment of a cyclic structure for the $[6\text{L}_1 + 12\text{Pd} + 6\text{L}_2]^{2+}$ ion. Compact ions have been shown to drift faster than ions with more extended structures upon ion-mobility separation;^[18] hence, the shoulder signal at 9.70 ms, which, based on its isotope spacing, also carries a +2 charge, is assigned to the linear $[6\text{L}_1 + 12\text{Pd} + 6\text{L}_2]^{2+}$ isomer. These findings and the fact that the ESI mass spectrum (Figure S1 in the Supporting Information) displays unique m/z values that correspond to hexameric species (e.g., m/z 3174), but no signals for pentameric and/or heptameric species, provide evidence that the macrocyclic structure **3** (Scheme 1) was indeed synthesized.

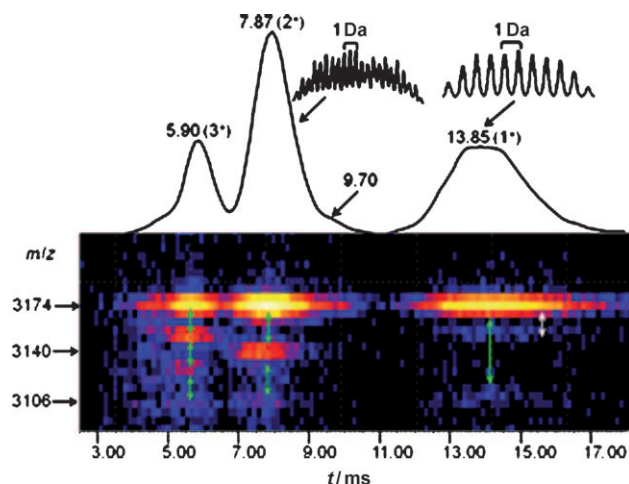


Figure 2. 2D ESI-TWIM-MS/MS plot for m/z 3174, acquired using a Waters Synapt quadrupole/time-of-flight (Q/TOF) mass spectrometer; m/z 3174 was mass-selected by Q for IM separation at a traveling wave height of 12 V and velocity of 350 m s^{-1} ; trap and transfer voltages were set at 6 V and 40 V, respectively (see the Supporting Information for complete experimental details). After separation, m/z 3174 gives rise to signals at 5.90, 7.87, and 13.85 ms, corresponding to triply charged aggregates (5.90 ms), cyclic $[6\text{L}_1 + 12\text{Pd} + 6\text{L}_2]^{2+}$ with 20 F^- and 2 BF_4^- counterions (7.87 ms) and linear species (13.85 ms). CAD with Ar, occurring in the transfer cell, causes losses of BF_3 and/or HF, which are indicated by green or white arrows respectively; m/z values of the fragments are marked on the y axis.

The stability of the macrocyclic architecture **3** was also examined by MS/MS. For this purpose, the ions at m/z 3174 were mass-selected and subjected to collisionally activated dissociation (CAD) experiments using argon in the trap cell, which is a collision cell located before the IM region, at collision energies ranging from 6 to 75 eV (Figure 3). The cyclic $[6\text{L}_1 + 12\text{Pd} + 6\text{L}_2]^{2+}$ species dissociate completely when the trap voltage reaches 75 V, which corresponds to a center-of-mass collision energy (E_{cm}) of 0.47 eV. Under equivalent experimental conditions, the E_{cm} value needed for complete fragmentation of $[6\text{L}_1 + 6\text{Cd}]^{2+}$, which is also macrocyclic,^[19] is 0.43 eV.

From the drift time of $[6\text{L}_1 + 12\text{Pd} + 6\text{L}_2]^{2+}$, an experimental collision cross section can be obtained by calibrating the drift time scale of the TWIM device with standards. Such a calibration was performed using the procedure of Scrivens and co-workers^[22] (Figure S7 in the Supporting Information) and led to a collision cross section of 601.7 \AA^2 for macrocycle **3**. However, the molecular architecture **3**, optimized by molecular mechanics/dynamics calculations (see Figure S4 and page S12 in the Supporting Information), leads to substantially larger cross sections. Specifically, the MOBCAL algorithm for cross sectional areas^[23] leads to cross sections of 1212.5 \AA^2 and 1388 \AA^2 with the projection approximation and exact hard-sphere scattering methods, respectively. Similarly, SIGMA^[24] and Driftscope 2.1^[25] algorithms give rise to 1309 \AA^2 and 1277.4 \AA^2 , respectively (both employ the projection approximation model). Substantial discrepancies between experimental and theoretical cross sections have been reported previously for the cyclic serine

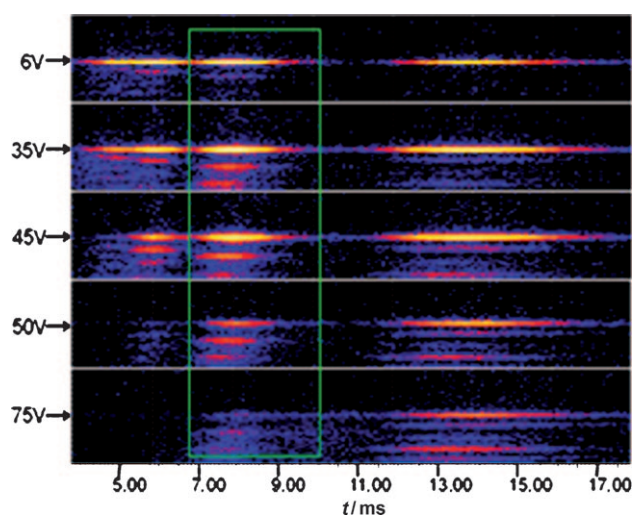


Figure 3. 2D ESI-TWIM-MS/MS plot of m/z 3174. The separated m/z 3174 components are indicated by arrows next to the trap cell voltages used for MS/MS. The signals for the $[6L_1 + 12Pd + 6L_2]^{2+}$ macrocycles are surrounded by a green rectangle.

(Ser) octamer,^[26] $[(Ser)_8 + H]^+$, the computationally predicted structure of which contains a large cavity, as does doughnut-shaped macrocycle **3**. In analogy to our results, the collision cross section of $[(Ser)_8 + H]^+$ obtained from ion-mobility experiments^[26a-d] was much smaller than the value derived from modeling studies.^[26e] The calculated cross-sectional areas for cationic crown ethers were found to be smaller than those measured by ion-mobility experiments.^[27] The algorithms used for modeling the geometries and cross sectional areas could be inadequate for large cyclic species that also contain sizable cavities, like our macrocycle or the serine octamer. A TWIM-MS study of metallomacrocycles of varying size (5-ring to 12-ring) is currently underway.

To further verify the structure of hexamer **3**, DOSY NMR experiments were conducted. The DOSY NMR shows only one species with a slow diffusion coefficient of $D = 3.07 \times 10^{-10} \text{ m}^2 \text{ s}^{-1}$, which gives a hydrodynamic radius of $r_H = 2.34 \text{ nm}$ (page S10 in the Supporting Information). This value corresponds well with a modeled average diameter of 5.2 nm.

UV/Vis spectra recorded for Pd complexes **2** and **3** (Table 1) in a dilute MeCN solution exhibit the expected absorption transitions; the signals that appeared below 300 nm were assigned to π - π^* transitions that arise from the heterocyclic ligands (terpy, 4,4'-bipy or 4-*tert*-butylpyridine), while the absorptions between 300 and 370 nm were assigned to metal-to-ligand charge-transfer (MLCT) transitions.^[28-30] The UV spectrum of **3** exhibited λ_{max} values at 240, 289, 336, and 366 nm, which had extinction coefficients (ϵ) that were 6.5, 5.6, 5.6 and 6.1 times larger, respectively, than the extinction coefficients of **2**.

Cyclic voltammograms (CV) of the precursor complex **2** and the Pd hexamer **3** in DMF are shown in Figure 4a and 4b, respectively; the corresponding potentials are listed in Table 2. For comparison, potentials for the free bis(terpyr-

Table 1: UV/Vis absorptions of the bis Pd adduct **2**. Values in parentheses are for complex **3**.

Complex	λ_{max} [nm]	ϵ [$10^3 \text{ M}^{-1} \text{ cm}^{-1}$]
2 , (3)	240 (240)	31 (207)
	289 (289)	28 (157)
	336 (336)	17 (98)
	366 (366)	10 (64)

idine) ligand (**1**), 4,4'-bipyridine, and Pd(COD)Cl₂ are also reported (cod = 1,5-cyclooctadiene).

Complex **2** shows two quasi-reversible reductions at -2.37 and -2.53 V , which can be assigned to two consecutive one-electron reduction processes of the bis(terpyridine) ligand; this assignment is based on the reduction potentials of the free bis(terpyridine) ligand **1** (Table 2). Complex **2** also shows an irreversible reduction at -1.06 V , which can be attributed to

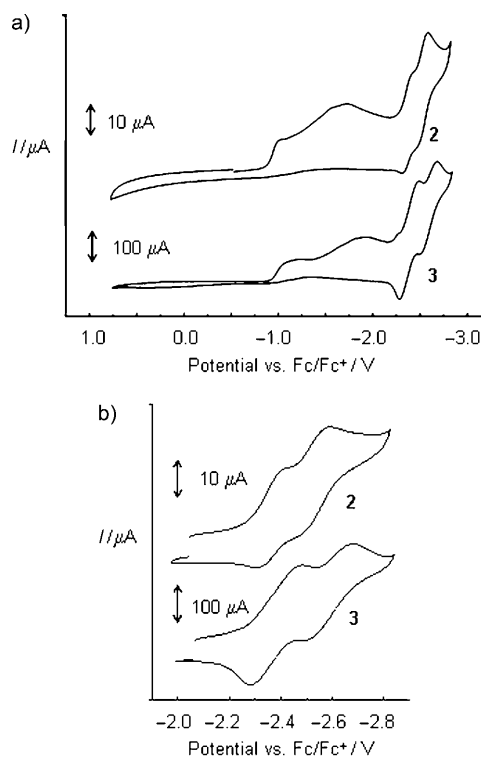


Figure 4. CV profiles of the bis Pd adduct **2** and hexamer **3**. The complete CV scans (a) and the expanded terpyridine-bipyridine regions (b) are depicted. Fc/Fc⁺ = ferrocene/ferrocenium.

Table 2: Redox potentials for complexes **2** and **3** along with related compounds.

Complex	Pd ²⁺ /Pd	4,4'-bpy	Bis(terpy)	
	$E_{1/2}$ [V]	$E_{1/2}$ [V]	$E_{1/2}(1)$	$E_{1/2}(2)$
bis(terpyridine) (1)			-2.42	-2.58
Pd bis(terpy) (MeCN) (2)	-1.06		-2.37	-2.53
Pd hexamer (3)	-1.20	-2.29	-2.38	-2.59
[Pd(cod)Cl ₂]	-1.05			
4,4'-bipyridine		-2.32		

the bielectronic reduction of the palladium cation coordinated to the bis(terpyridine) ligand; CV of the Pd(cod)Cl₂ complex shows a reduction wave at a similar potential. The broad irreversible wave at approximately -1.75 V has not been assigned.

The CV profiles for complex **2** and Pd hexamer **3** are similar (Figure 4), thus indicating a similar electrochemical behavior. Complex **3** also exhibits two quasi-reversible reductions corresponding to the bis(terpyridine) ligand and one irreversible reduction that is assigned to the two-electron reduction of the Pd^{II} ion. Reduction of the 4,4'-bipyridine ligand was also expected to occur in complex **3**. The free bipyridine ligand exhibits a reduction potential of -2.32 V. In complex **3**, this reduction is very close to the first reduction of the bis(terpyridine) ligand. Specifically, the bipyridine reduction is detected at -2.29 V in the cathodic wave; however, in the anodic wave, it overlaps with the first reduction of the bis(terpyridine) ligand, and appears at a somewhat more positive potential than what would be expected for only the first bis(terpyridine) reduction.

A closer look at the first and second reduction potentials for the bis(terpyridine) ligands of complexes **2** and **3** (Figure 4b) reveals that the reduction processes for complex **3** lead to larger currents. Further, the anodic to cathodic peak separation within each reduction process is almost twice as large for complex **3** than complex **2**, thus indicating that the quasi-reversible electrochemical processes of complex **3** are less reversible than that of complex **2** (see Table S3 in the Supporting Information); notably, a less reversible redox process is characterized by signals that are reduced in size and more separated (compared to a more reversible process); this effect is postulated^[31] to arise from a larger structural reorganization. The higher current intensity for complex **3** as compared to the Pd adduct **2** (see Table S3 in the Supporting Information), can be explained by the larger number of electrons exchanged in each reduction step; with the hexameric complex **3**, simultaneous reduction of all six identical non-interacting Pd bis(terpyridine) units can occur.

In conclusion, we have demonstrated the assembly of a dodeca Pd^{II} terpyridine based macrocycle (**3**) using the Pd^{II} bis(terpyridine) adduct **2** and 4,4'-bipyridine. This hexameric metallomacrocycle has been successfully characterized using ESI-TWIM-MS, which enabled the detection of distinct supramolecular isomers. Tandem mass spectrometry experiments revealed that the Pd^{II} macrocycle dissociates less readily than linear architectures, which is consistent with the need to break more bonds in the fragmentation of a cyclic structure compared with a linear species. The use of ESI-TWIM-mass spectrometry for the study of higher order supramolecular architectures is ongoing.

Received: November 3, 2009
 Revised: June 16, 2010
 Published online: July 28, 2010

Keywords: DOSY NMR spectroscopy · macrocycles · mass spectrometry · palladium · supramolecular chemistry

- [1] I. Eryazici, P. Wang, C. N. Moorefield, M. Panzer, M. Durmas, C. D. Shreiner, G. R. Newkome, *Dalton Trans.* **2007**, 626–628.
- [2] R. Trokowski, S. Akine, T. Nabeshima, *Chem. Commun.* **2008**, 889–890.
- [3] S.-H. Hwang, C. N. Moorefield, F. R. Fronczek, O. Lukoyanova, L. Echegoyen, G. R. Newkome, *Chem. Commun.* **2005**, 713–715.
- [4] F. M. Romero, R. Ziessel, A. Dupont-Gervais, A. Van Dorsselaer, *Chem. Commun.* **1996**, 551–553.
- [5] E. C. Constable, C. E. Housecroft, C. B. Smith, *Inorg. Chem. Commun.* **2003**, 6, 1011–1013.
- [6] J. D. Crowley, A. J. Goshe, B. Bosnich, *Chem. Commun.* **2003**, 2824–2825.
- [7] R. D. Sommer, A. L. Rheingold, A. J. Goshe, B. Bosnich, *J. Am. Chem. Soc.* **2001**, 123, 3940–3952.
- [8] J. D. Crowley, I. M. Steele, B. Bosnich, *Eur. J. Inorg. Chem.* **2005**, 3907–3917.
- [9] A. J. Goshe, B. Bosnich, *Synlett* **2001**, 0941–0944.
- [10] S. H. Hwang, P. Wang, C. N. Moorefield, L. A. Godínez, J. Manriquez, E. Bustos, G. R. Newkome, *Chem. Commun.* **2005**, 4672–4674.
- [11] G. R. Newkome, T. J. Cho, C. N. Moorefield, P. P. Mohapatra, L. A. Godínez, *Chem. Eur. J.* **2004**, 10, 1493–1500.
- [12] G. R. Newkome, T. J. Cho, C. N. Moorefield, R. Cush, P. S. Russo, L. A. Godínez, M. J. Saunders, P. Mohapatra, *Chem. Eur. J.* **2002**, 8, 2946–2954.
- [13] G. R. Newkome, T. J. Cho, C. N. Moorefield, G. R. Baker, M. J. Saunders, R. Cush, P. S. Russo, *Angew. Chem.* **1999**, 111, 3899–3903; *Angew. Chem. Int. Ed.* **1999**, 38, 3717–3721.
- [14] I. Eryazici, C. N. Moorefield, S. Durmus, G. R. Newkome, *J. Org. Chem.* **2006**, 71, 1009–1014.
- [15] T. Mutai, J. D. Cheon, S. Arita, K. Araki, *J. Chem. Soc., Perkin Trans. 2* **2001**, 1045–1050.
- [16] a) P. Wang, G. R. Newkome, C. Wesdemiotis, *Int. J. Mass Spectrom.* **2006**, 255–256, 86–92; b) K. Ghosh, J. Hu, H. S. White, P. J. Stang, *J. Am. Chem. Soc.* **2009**, 131, 6695–6697; c) M. Wang, Y. R. Zheng, K. Ghosh, P. J. Stang, *J. Am. Chem. Soc.* **2010**, 132, 6282–6283; d) S. Sakamoto, M. Fujita, K. Kim, K. Yamaguchi, *Tetrahedron* **2000**, 56, 995; e) S. Sato, Y. Ishido, M. Fujita, *J. Am. Chem. Soc.* **2009**, 131, 6064–6065; f) C. A. Schalley, T. Müller, P. Linnartz, M. Witt, M. Schäfer, A. Lützen, *Chem. Eur. J.* **2002**, 8, 3538–3551; g) M. Engeser, A. Rang, M. Ferrer, A. Gutiérrez, H. T. Baytekin, C. A. Schalley, *Int. J. Mass Spectrom.* **2006**, 255–256, 185–194; h) W. Jiang, A. Schäfer, P. C. Mohr, C. A. Schalley, *J. Am. Chem. Soc.* **2010**, 132, 2309–2320; i) B. Bocquet, G. Bernardinelli, N. Ouali, S. Floquet, F. Renaud, G. Hopfgartner, C. Piguet, *Chem. Commun.* **2002**, 930–931.
- [17] S. D. Pringle, K. Giles, J. L. Wildgoose, J. P. Williams, S. E. Slade, K. Thalassinou, R. H. Bateman, M. T. Bowers, J. H. Scrivens, *Int. J. Mass Spectrom.* **2007**, 261, 1–12.
- [18] a) M. T. Bowers, P. R. Kemper, G. von Helden, P. A. M. van Koppen, *Science* **1993**, 260, 1446–1451; b) D. E. Clemmer, M. F. Jarrold, *J. Mass Spectrom.* **1997**, 32, 577–592; c) C. S. Hoaglund-Hyzer, A. E. Counterman, D. E. Clemmer, *Chem. Rev.* **1999**, 99, 3037–3079; d) G. F. Verbeck, B. T. Ruotolo, H. A. Sawyer, K. J. Gillig, D. H. Russel, *J. Biomol. Tech.* **2002**, 13, 56–61; e) L. S. Fenn, J. A. McLean, *Anal. Bioanal. Chem.* **2008**, 391, 905–909; f) B. T. Ruotolo, J. L. P. Benesch, A. M. Sandercock, S.-J. Hyung, C. V. Robinson, *Nat. Protoc.* **2008**, 3, 1139–1152; g) A. B. Kanu, P. Dwivedi, M. Tam, L. Matz, H. H. Hill, *J. Mass Spectrom.* **2008**, 43, 1–22; h) S. Trimpin, D. I. Plasencia, D. E. Clemmer, *Anal. Chem.* **2007**, 79, 7965–7974; i) S. Trimpin, D. E. Clemmer, *Anal. Chem.* **2008**, 80, 9073–9083; j) G. R. Hilton, A. T. Jackson, K. Thalassinou, J. H. Scrivens, *Anal. Chem.* **2008**, 80, 9720–9725;

- k) A. P. Gies, M. Kliman, J. A. McLean, *Macromolecules* **2008**, *41*, 8299–8301.
- [19] Y.-T. Chan, X. Li, M. Soler, J.-L. Wang, C. Wesdemiotis, G. R. Newkome, *J. Am. Chem. Soc.* **2009**, *131*, 16395–16397.
- [20] S. H. Hwang, C. N. Moorefield, P. Wang, J. Y. Kim, S. W. Lee, G. R. Newkome, *Inorg. Chim. Acta* **2007**, *360*, 1780–1784.
- [21] J. Wang, *Analytical Electrochemistry*, Wiley, New York, **2006**.
- [22] K. Thalassinou, M. Grabenauer, S. E. Slade, G. R. Hilton, M. T. Bowers, J. H. Scrivens, *Anal. Chem.* **2009**, *81*, 248–254.
- [23] Available at <http://www.indiana.edu/~nano/software.html>.
- [24] Available at http://bowers.chem.ucsb.edu/theory_analysis/cross-sections/index.shtml.
- [25] Software for the analysis of ion mobility data, available from Waters Inc., Milford, MA (<http://www.waters.com/>).
- [26] a) R. G. Cooks, D. Zhang, K. J. Koch, F. C. Gozzo, M. N. Eberlin, *Anal. Chem.* **2001**, *73*, 3646–3655; b) Z. Takats, S. C. Nanita, G. Schlosser, K. Vekey, R. G. Cooks, *Anal. Chem.* **2003**, *75*, 6147–6154; c) P. Yang, R. Xu, S. C. Nanita, R. G. Cooks, *J. Am. Chem. Soc.* **2006**, *128*, 17074–17086; d) S. C. Nanita, R. G. Cooks, *Angew. Chem. Int. Ed.* **2006**, *45*, 554–569; e) A. E. Counterman, D. E. Clemmer, *J. Phys. Chem. B* **2001**, *105*, 8092–8096.
- [27] A. A. Shvartsburg, B. Liu, K. W. M. Siu, K.-M. Ho, *J. Phys. Chem. A* **2000**, *104*, 6152–6157.
- [28] L. Barloy, R. Gauvin, J. Osborn, C. Sizun, R. Graff, N. Kyritsakas, *Eur. J. Inorg. Chem.* **2001**, 1699–1707.
- [29] E. M. Ratilla, H. M. Brothers, N. M. Kostic, *J. Am. Chem. Soc.* **1987**, *109*, 4592–4599.
- [30] H. M. Brothers, N. M. Kostic, *Inorg. Chem.* **1988**, *27*, 1761–1767.
- [31] W. Zhang, C. Bensimon, R. J. Crutchley, *Inorg. Chem.* **1993**, *32*, 5808–5812.
-